

Synthesis, spectroscopic, and electronic properties of new tetrapyrazinoporphyrazines with eight peripheral 2,6-diisopropylphenol groups

Benjamin Marx^a, Briana R. Schrage^{a,◊,†}, Christopher J. Ziegler^{b,◊} and Victor N. Nemykin^{a,◊,*}

^aDepartment of Chemistry, University of Tennessee – Knoxville, Knoxville, TN, 37996, USA

Received 6 October 2022 Accepted 6 December 2022

Dedicated to Prof. Tomás Torres on the occasion of his 70th birthday

ABSTRACT: Metal-free, magnesium, titanyl, and vanadyl tetrapyrazinoporphyrazines substituted with eight 2,6-diisopropylphenoxy groups at the peripheral positions were prepared and characterized by NMR, UV-Vis, magnetic circular dichroism (MCD), and mass spectrometry methods. In addition, the Pc^{(2,6iPrPhO)8}VO complex was characterized by EPR spectroscopy and X-ray crystallography. Reaction between TiCl₄ with 4,5-(2,6-diisopropylphenoxy)phthalonitrile in N,N-dimethylaminoethanol resulted in the formation of a red open-chain trimer, which was characterized by mass spectrometry and X-ray crystallography. Electronic structures of new compounds and their excited state properties were probed by Density Functional Theory (DFT) and Time-Dependent DFT (TDDFT) methods.

KEYWORDS: tetrapyrazinoporphyrazine, X-ray crystallography, MCD spectroscopy, DFT, and TDDFT calculations.

INTRODUCTION

Phthalocyanines and their analogs are well-known synthetic dyes used in the textile and ink industries [1]. In addition, these brightly colored molecules are also used in catalysis [2], photodynamic therapy [3], optical imaging and bioimaging [4], semiconducting devices [5], and light harvesting modules for organic photovoltaics [6]. The ease of preparation and ability to fine-tune the magnetic and optical properties of phthalocyanines are key to their popularity among the scientific community [7]. It has been demonstrated by Hadt and coworkers that the unsubstituted vanadyl phthalocyanine diluted by

titanyl phthalocyanine as well as copper phthalocyanine diluted by zinc phthalocyanine can be viewed as viable candidates for applications in quantum computing [8]. One of the disadvantages of using paramagnetic phthalocyanines in spintronic applications is the strong intermolecular packing forces observed in their crystal lattices. Indeed, independently of the phase, all unsubstituted phthalocyanines form close non-covalent packing with the typical phthalocyanine to phthalocyanine distance of about 3.3 Å [9]. Such strong π - π interactions lead to small metal-metal distances between neighboring phthalocyanine molecules in the solid state. This in turn dramatically reduces the spin coherence time in these systems. In order to improve spin coherence times, paramagnetic phthalocyanines need to be significantly diluted by diamagnetic hosts [8]. Although such dilution improves spin coherence times, it also reduces spin densities per cubic volume. One of the possible strategies to improve spin coherence while maintaining high spin densities per unit

^bDepartment of Chemistry, University of Akron, Akron, OH, 44325, USA

^oSPP full member in good standing.

^{*}Correspondence to: Victor N. Nemykin, e-mail: vnemykin@utk.edu

[†]Current address: Oakridge National Laboratory, Knoxville, USA.

volume could be to use phthalocyanines and their analogues with bulky substituents that prevent aggregation [10]. As was demonstrated by McKeown and coworkers, phthalocyanines and tetrapyrazinoporphyrazines substituted by eight 2,6-diisopropylphenoxy groups form a unique solid-state crystal structure that consists of macrocycle boxes with large pores that are formed as a result of specific non-covalent interactions between hydrophobic isopropyl groups [11]. Because Hadt and coworkers have demonstrated that the vanadyl phthalocyanine diluted by titanyl phthalocyanine outperformed at room temperature the copper/zinc pair [8], we have explored synthetic strategies for the preparation of the titanyl and vanadyl tetrapyrazinoporphyrazines substituted by eight 2,6-diisopropylphenoxy groups.

EXPERIMENTAL

General

All chemicals were purchased from commercial sources. Solvents were purified using standard procedures. Jasco-V770 spectrophotometer was used to collect UV-Vis data. All MCD spectra were collected using a Jasco V-1500 spectropolarimeter. NMR spectra were recorded by a Bruker Avance instrument with a 300 MHz frequency for protons and a 75 MHz frequency for carbons. Chemical shifts are reported in parts per million (ppm) and referenced to the residual proton resonance of the deuterated solvent (CDCl₃ = δ 7.26) and carbon spectra are referenced to the carbon resonances of the solvent (CDCl₃ = δ 77.16). High-resolution mass spectra of all new compounds were recorded using a Bruker micrOTOF-QIII. All exact mass measurements showed an error of less than 5 ppm. Fluorescence emission data in solution were recorded on a Horiba PTI QuantaMaster 8000 fluorescence spectrophotometer using Rhodamine 6G in EtOH as a standard. All slit widths were held constant at 2 nm. The quantum yields in solution were calculated using the following equation:

$$\Phi_X = \Phi_{ST} \left(\frac{Grad_X}{Grad_{ST}} \right) * \left(\frac{v_X^2}{v_{ST}^2} \right)$$

 $\eta_{ST} = 1.361$, $\Phi_{ST} = 0.94$; $\eta_X = 1.424$ (2), and *Grad* the gradient from the plot of integrated fluorescence intensity vs absorbance. EPR spectra were collected on a Bruker X-band ELEXSYS E-500 instrument at 150 K. Samples were prepared and frozen under a nitrogen atmosphere.

DFT and TDDFT calculations

All calculations were run using Gaussian 16 [12]. TPSSh exchange-correlation functional [13,14] with Wachter's full-electron basis set [15] for transition metals and the 6-311G(d) basis set [16] for the other atoms

was used for all geometry optimizations. Vibrational frequencies were calculated to ensure all geometries were local minima. M06 [17] functional was used in single-point and TDDFT calculations with the same basis sets. QMForge [18] was used for molecular orbital composition analyses.

X-ray crystallography

X-ray quality crystals of vanadyl complex 2 were obtained by slow diffusion of methanol into the DCM/ acetonitrile solution of 2. Crystals of 3 were obtained by slow diffusion of methanol into the DCM/toluene solution of 3. X-ray data for complex 2 and open-chain trimer 3 were collected with a Cu microsource on a Bruker D8 Venture diffractometer at 100 K using an Oxford Cryostream low-temperature apparatus. Experimental data sets were reduced with Bruker SAINT. Absorption correction was done using SADABS. Structures were solved using Superflip [19] or SHELXS [20] and refined using Crystals for Windows program [21]. Disordered water and acetonitrile solvents observed in the pores of compound 2 were eliminated with PLATON SQUEEZE [22] procedure. Complete structural data on 2 can be accessed using CCDC reference number 2208789 and is also available in the Supporting Information. The crystals for the open-chain compound 3 were too small and thus the best dataset only allowed the refinement of the structure using isotropic spheres (R ~32%). Thus, this structure was used only to establish the connectivity in the molecule and was not deposited to the CCDC database although the CIF is available from the authors on request.

Synthesis

Preparation of 5,6-Bis(2,6-diisopropylphenoxy)pyrazine-2,3-dicarbonitrile (1): Compound 1 was prepared according to a previously published procedure by Novakova and coworkers [23].

Preparation of vanadyl tetrapyrazinoporphyrazine (2): Compound 1 (1.002 g, 2.076 mmol), vanadium trichloride (0.5 equiv), and a scoop of urea was dissolved in dry N,N-dimethylaminoethanol (2 mL) in an argon atmosphere and boiled for 4 hrs. Upon cooling, deionized water (100 mL) was added to the reaction mixture and the resulting precipitate was collected and washed thoroughly with more water. The solid was purified by means of a silica plug eluting with 3:1 DCM/acetone then further washed with 1:1 water/methanol and pure methanol to give a green solid in 59% yield (1.236 g). UV-Vis (DCM): $λ_{max}$ (ε) = 634 nm (91,880 M⁻¹ cm⁻¹). HRMS (MALDI-TOF, positive mode) m/z: calcd for $C_{120}H_{137}N_{16}O_9V$ 1998.0226, found 1998.0215 [M+H]⁺.

Preparation of trimeric linear product (3): N,N-Dimethylaminoethanol (2 mL) was purged with argon in a Schlenk flask, titanium tetrachloride (0.5 equiv) was then added via syringe, and the resultant fumes allowed to

completely evolve. Compound 1 (414 mg, 0.858 mmol) was added and the resultant mixture was heated to ~100 °C for 3 hrs. Upon cooling, the purple solution was poured into deionized water (100 mL) and the precipitate was filtered. The crude product was purified by silica gel column chromatography eluting with DCM to give a small amount (a few milligrams) of a red solid. $\lambda_{max} = 556$ nm. HRMS (MALDI-TOF, positive mode) m/z calcd for $C_{90}H_{105}N_{11}O_8$ 1467.8148, found 1467.8110 [M]⁺.

Preparation of titanyl tetrapyrazinoporphyrazine (4): Compound 1 was stirred in dry quinoline (3 mL) in an argon atmosphere for ~ 10 mins and then titanium tetrachloride (0.5 equiv) was added and the resulting mixture heated to 150-160 °C for 1 hr. Upon cooling, the green solution was poured into 1:1 MeOH/deionized water and the precipitate filtered off, which then was further washed with the same ratio (200 mL) as well as 8:2 MeOH/water (400 mL). The product was dissolved in DCM and filtered through a membrane frit to remove the titanium dioxide byproduct and evaporated to give a green solid in 36% yield (0.416 g). ¹H NMR $(500 \text{ MHz}, \text{CDCl}_3)$: $\delta = 7.63 \text{ (t, 8H)}, 7.48 \text{ (d, 16H)}, 3.33$ (m, 16H), 1.38 (d, 93H). 13C NMR (125 MHz, CDCl₃): $\delta = 152.95, 147.84, 147.79, 141.90, 141.15, 140.22,$ 127.02, 124.66, 28.42, 23.67. UV-Vis (DCM): λ_{max} (ϵ) = 635 nm (120,693 M⁻¹ cm⁻¹). HRMS (MALDI-TOF, positive mode) m/z: calcd for C₁₂₀H₁₃₇N₁₆O₉Ti 1995.0271, found 1995.0270 [M+H]+.

Preparation of magnesium tetrapyrazinoporphyrazine (5): Magnesium ribbon (55 mg, 2.3 mmol) with a catalytic amount of iodine was refluxed in dry N,Ndimethylaminoethanol (3 mL) for 1 hr under an argon atmosphere. Compound 1 (2.18 g, 4.6 mmol) was added and the mixture was refluxed for 6 hrs. After cooling, the mixture was poured into 1:1 MeOH/deionized water (100 mL) and the resulting precipitate filtered. The solid was further washed with increasing amounts of MeOH/ water up to a 9:1 ratio. The product was purified by silica gel column chromatography eluting with 4:1 DCM/acetone to give a cyan solid in 34% yield (1.49 g). ¹H NMR $(500 \text{ MHz}, \text{CDCl}_3)$: $\delta = 7.55 \text{ (t, 8H)}, 7.42 \text{ (d, 16H)}, 3.30$ (m, 16H), 1.28 (d, 96H). 13C NMR (125 MHz, CDCl₃): $\delta = 151.67, 149.91, 148.09, 142.59, 141.23, 126.77,$ 124.53, 28.27, 23.62. UV-Vis (DCM): λ_{max} (ϵ) = 630 nm (104,864 M⁻¹ cm⁻¹). HRMS (MALDI-TOF, positive mode) m/z: calcd for C₁₂₀H₁₃₇N₁₆O₈Mg 1955.0685, found 1955.0693 [M]+.

Preparation of metal free tetrapyrazinoporphyrazine (6): Compound 5 was dissolved in equal parts (5 mL) dry THF and acetic acid and heated at 75 °C for 2 hr. After cooling, the mixture was poured into deionized water (150 mL) and the precipitate filtered. The solid was thoroughly washed with water and methanol and then purified by silica gel column chromatography eluting with DCM then 4:1 DCM/MeOH to give a cyan solid in 52% yield (0.763 g). ¹H NMR (500 MHz,

CDCl₃): δ = 7.59 (t, 8H), 7.45 (d, 16H), 3.32 (m, 16H), 1.32 (d, 96H), -2.09 (bs, 2H, NH). ¹³C NMR (125 MHz, CDCl₃): δ = 152.33, 147.98, 141.25, 141.19, 126.85, 124.59, 28.38, 23.66. UV-Vis (DCM): λ_{max} (ϵ) = 649 nm (94,058 M⁻¹ cm⁻¹). HRMS (MALDI-TOF, positive mode) m/z: calcd for C₁₂₀H₁₃₉N₁₆O₈ 1933.0992, found 1933.0969 [M+H]⁺.

RESULTS AND DISCUSSION

Both titanyl and vanadyl tetrapyrazinoporphyrazines outlined in Scheme 1 were not reported previously. The direct reaction between pyrazinedicarbonitrile 1 and vanadium trichloride in boiling N,N-dimethylaminoethanol (DMAE) results in the formation of a green-colored reaction mixture which after the standard purification steps (see the experimental section for details) leads to the isolation of pure vanadyl tetrapyrazinoporphyrazine 2. A similar reaction with titanium tetrachloride leads to a dark purple solution. Based on the UV-Vis spectrum, this solution has no desired titanyl complex 4 but consists of several open-chain oligomers. Based on the mass spectrum and X-ray data, one of the oligomers was identified as the trimeric linear subunit 3. The use of titanium butoxide instead of TiCl₄ also does not lead to the desired macrocycle product. The reaction of the pyrazinedicarbonitrile 1 with titanium butoxide in bromonaphthalene also does not lead to the desired product 4. However, the reaction between nitrile 1 and titanium tetrachloride in boiling quinoline showed the initial formation of a green color that disappeared upon further refluxing. Optimization of the synthesis of desired complex 4 was obtained by varying reaction temperature and time. Under the optimized conditions, product 4 was obtained in the reaction between pyrazinedicarbonitrile 1 with titanium tetrachloride in quinoline at ~ 150 °C for 1 hour. Alternatively, we thought that complex 4 could be formed by the interaction of the metal-free tetrapyrazinoporphyrazine 6 with titanium tetrachloride or titanium butoxide. In turn, the metal-free tetrapyrazinoporphyrazine 6 can be formed by demetalation of magnesium complex 5 with a large excess of acetic acid. Magnesium complex 5 can be prepared from nitrile 1 and magnesium alkoxide in boiling DMAE. Using this strategy, we have prepared magnesium complex 5 without any issues in reasonable yield. Using a large excess of acetic acid, compound 5 was transformed into metalfree species [6H_n]ⁿ⁺, protonated at the nitrogen atoms. Clean deprotonation of this compound was challenging and required the use of triethylamine or stronger bases. Once formed, metal-free complex 6 was tested in the metalation reaction with titanium tetrachloride and titanium butoxide. Despite testing several different reaction conditions, we were not able to see the formation of the desired titanyl complex 4 in reasonable yield. Thus in our hands, the direct formation of the desired titanyl

Scheme 1. Synthetic route for the preparation of target compounds 2-6.

complex 4 in the reaction between nitrile 1 and titanium tetrachloride in hot quinoline was found to be the optimal reaction condition.

The UV-Vis and MCD spectra of these new macrocycles are shown in Fig. 1. As expected [24], the metal complexes have one characteristic Q-band, while the lowering of symmetry from D_{4h} to D_{2h} in the metal-free compound leads to the splitting of the Q-band into Qx and Q_v components. The Soret band in all four macrocycles can be found in the 350 nm region. In addition, in the titanyl, vanadyl, and metal-free compounds, a prominent band is found in the 420 nm region, which has a significant charge-transfer character (see TDDFT calculations discussion below) [25]. This band is also present in the magnesium complex, although at a significantly lower intensity, which might be reflective of the higher symmetry of this compound. In the MCD spectra, the Q-band observed for the metal-containing macrocycles is associated with a very strong MCD A-term centered at an energy close to the energy of the observed Q-band. In the case of the metal-free compound, the Q-band region is associated with five observable B-terms located at 649, 628, 611, 591, and 559 nm. As expected, the Soret band is associated with the observed A-term centered in the 350 nm region. In addition, an A-term has been observed in the 400-450 nm region of the MCD spectrum. This term is associated with absorption centered in this region. In general, the Q-band in compounds 2, 4-6 is blue-shifted compared to the phthalocyanine

analogs which is typical of tetrapyrazinoporphyrazino complexes. No fluorescence has been observed for the open-shell vanadyl complex, while the fluorescence of the titanyl, magnesium, and metal-free compounds are shown in Fig. 1 along with the fluorescence spectrum of the open-chain trimer. These spectra are typical for tetrapyrazinoporphyrazino compounds and other chromophores and are mirror images of the lowest energy absorption bands. Their quantum yields were also found in the expected range (Fig. 1).[10e,11] High-resolution mass spectra of all compounds are in good agreement with the expected formula (Supporting Information). The ¹H NMR spectra of titanyl, magnesium, and metalfree compounds show the expected patterns for all protons although the methyl groups for the titanyl complex were found to be diastereotopic (Supporting Information). 13C NMR spectra for all prepared compounds agree with their associated structures (Supporting Information). The EPR spectrum of vanadyl complex 2 is shown in Fig. 2. As expected, it has an axial symmetry and parameters that correlate well with the $s = \frac{1}{2} (d_{xy})^{1}$ electronic configuration of this complex ($g_L = 1.98$, g_{\parallel} = 1.96, A_L = 175 MHz, and A_{\parallel} = 430 MHz). IR spectra of all macrocyclic compounds are shown in Supporting Information. Because of the high porosity of the crystalline macrocyclic complexes (Fig. 3 and reference 11), their IR spectra tend to contain strong signals of the residual solvents. However, when samples were dried at 80°C in a vacuum for several hours, the IR spectra were

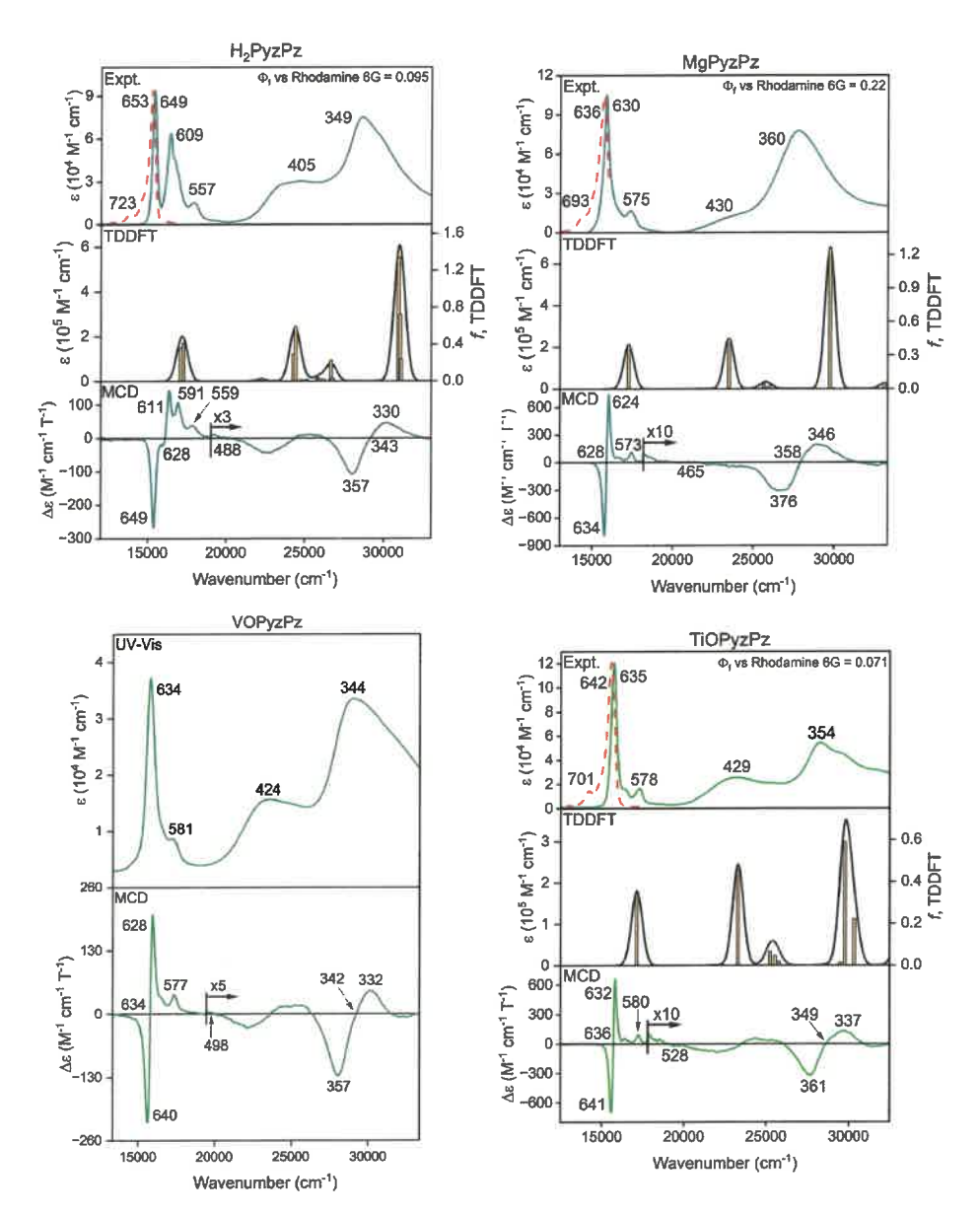


Fig. 1. Experimental UV-Vis (solid), MCD, and fluorescence (dashed) spectra of the target compounds along with their TDDFT-predicted absorption spectra.

consistent with those reported by Zimcik and co-authors for 5 and 6.

The X-ray crystal structures of the vanadyl complex and linear red trimer are shown in Fig. 3. The unit cell of the vanadyl complex 2 is isostructural with the iron and cobalt analogs previously reported by McKeown and coworkers [11]. It crystallizes in orthorhombic primitive cells with a length of 37.26760(6) Å. The nanopore structure of vanadyl complex 2 consists of tetrapyrazinoporphyrazine dimers. Each monomeric unit has V=O fragment disordered over the tetrapyrazinoporphyrazine plane. These fragments form the nanoporous structure with walls constructed by four such dimers. The nanostructure's porous parameters are similar to

the previously reported iron and cobalt analogs [11]. Although McKeown and coauthors mention that the presence of the bidentate ligand (so-called wall ties) in the iron and cobalt structures is critical for the formation of the nanoporous walls and maintaining stability [11], the lack of such bidentate ligand in our vanadyl complex indicates that the hydrophobic isopropyl group interactions can play at least as significant role as the bidentate ligands. The large intermolecular distances of the cavity (about 3.7 nm) are critical for the application of the vanadyl and titanyl complexes in spintronics as it is expected that titanyl complex 4 will crystallize in a similar phase. The low quality of the crystal structure for the red trimer 3 precludes definitive elucidation of the terminal groups.

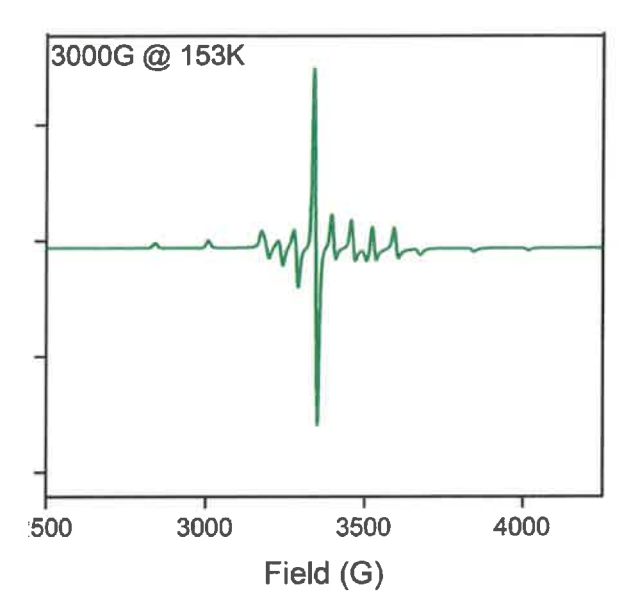


Fig. 2. EPR spectrum of vanadyl complex **2** in frozen solution (DCM:THF 50:50 v/v) at 153K.

However, the crystallographically determined C=O bond distance is ~1.20 Å, which are characteristic for C=O double rather than imine group. Again, because of the small size of the crystals, we were not able to refine this crystal structure and only used it here to prove the connectivity in 3. From a molecular connectivity point of view (Fig. 3d), it is clear that the driving force for the formation for the red trimer is the presence of strong hydrogen bonds between N-H fragments of the outer subunits and the pyrazine nitrogen atoms located in the central sububit.

The electronic structure and nature of the excited states in all macrocyclic complexes were probed by density

functional theory (DFT) and time-dependent density functional theory (TDDFT) calculations. The energy diagram of the compounds (2-6) and select images of their frontier orbitals are given in Figs. 4, 5, Supporting Information as well as in Table 1. First, we need to mention that all geometry optimizations, single point, and TDDFT calculations, were conducted on the full structures of 2-6. In these cases, the optimized geometry is indicative of the perpendicular orientation of 2,6-diisopropylphenoxy groups concerning the macrocyclic plane which agrees well with all known X-ray crystal structures of this system [11]. On the contrary, the usual truncation of the isopropyl groups from the initial structure of 2-6 leads to optimized geometries in which one of the phenoxy groups becomes fully conjugated with the macrocycle. Such conjugation is expected for phthalocyanines and their analogs with sterically unhindered aromatic substituents. Thus, optimization of the full structures (2-6) results in reasonable geometries. The DFT predicted HOMO for complexes 2-6 resembles the Gouterman [26] a_{1u} (in a standard D_{4h} point group notation) orbital. The LUMO and LUMO+1 in all compounds resemble Gouterman's pair of e_a orbitals. In the case of the vanadyl complex 2, the HOMO-1 (\alpha-set) is a vanadyl-centered d_{vv} orbital, which agrees well with the observed EPR spectrum of this compound. The classic Gouterman's $a_{2\mu}$ orbital in all macrocycles is well separated from the frontier orbitals energies and was predicted to be the HOMO-21 in the metal derivatives and HOMO-23 in the metal-free 6. However, the HOMO-2 also has an a_{2u} symmetry although it has no electron density on the inner nitrogen atoms and has a substantial contribution from the phenoxy groups (Fig. 5).

Taking into consideration the large size of the systems and the necessity to use a large basis set for the prediction

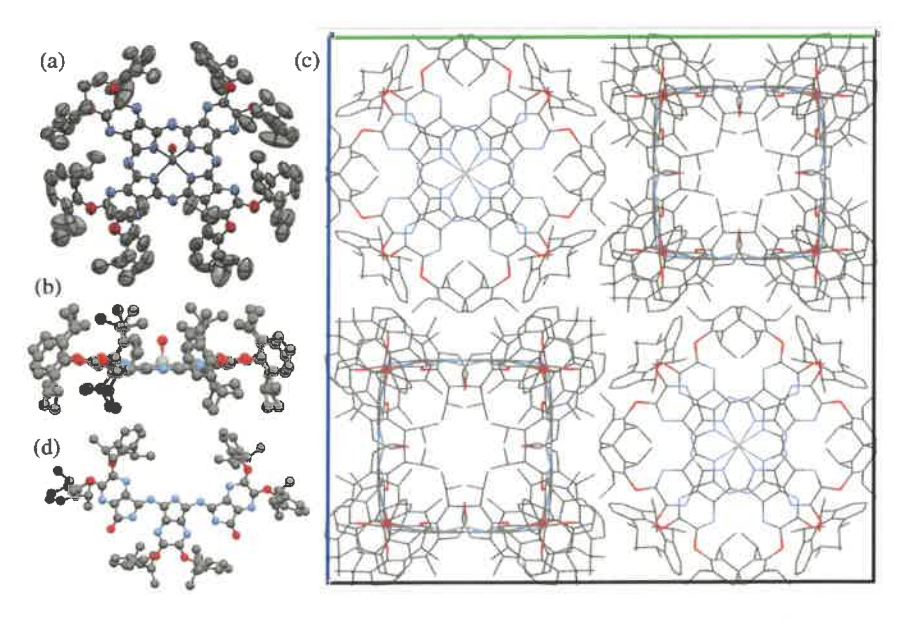


Fig. 3. X-ray crystal structure of complex 2 (a-c) and trimer 3 (d); (a): top view of 2; (b) side view of 2; (c) packing diagram for 2.

Table 1. DFT-predicted (M06 functional) composition for the selected MOs in macrocyclic compounds **2**, **4-6**.

МО	Energy/eV	% M (M=O)	% PyzPz Core	% Phenoxy
VOPyzI	Pz (α-set, 2)			
H-3	-6.882	1.24	33.98	64.78
H-2	-6.881	0.64	37.24	62.12
H-1	-6.661	62.16	36.67	1.18
номо	-5.989	0	94.70	5.29
LUMO	-3.409	2,29	91.70	6.01
L+1	-3.409	2.29	91.70	6.01
L+2	-1.946	3.10	66.91	29.99
L+3	-1.819	7.15	58.17	34.68
VOPyzP	Pz (β-set, 2)			
H-4	-6.891	0.89	30.77	68.34
H-3	-6.891	0.89	30.77	68.34
H-2	-6.881	0.54	37.42	62.04
H-1	-6.871	0.08	36.85	63.06
номо	-5.978	0.00	94.72	5.27
LUMO	-3.409	1.67	92,23	6.11
L+1	-3.409	1.67	92.23	6.11
L+2	-1.905	1.10	66.79	32.11
L+3	-1.785	4.23	59.47	36.29
TiOPyzl	Pz (4)			
H-21	-7.896	11.22	86.29	2.50
H-4	-6.898	1.21	31.34	67.45
H-3	-6.898	1.21	31.34	67.45
H-2	-6.896	0.57	35.53	63.90
H-1	-6.883	0.08	35.94	63.98
номо	-6.045	0	94.67	5.32
LUMO	-3.460	1.43	92.63	5.94
L+1	-3.460	1.43	92.63	5.94
L+2	-2.304	57.07	42.49	0.44
L+3	-1.934	1.41	67.07	31.52
MgPyzP	z (5)			
H-21	-7.666	1.74	96.44	1.82
H-4	-6.820	0	40.82	59.17
H-3	-6.820	0	40.82	59.17
H-2	-6.815	0.15	41.90	57.95
H-1	-6.776	0	48.69	51.31
номо	-5.886	0	94.85	5.15
LUMO	-3.287	0	94.23	5.77
L+1	-3.287	0	94.23	5.77
L+2	-1.731	0	65.67	34.33
L+3	-1.655	1.53	60.83	37.64
				(Continued)

(Continued)

Table 1. (Continued)

МО	Energy/eV	% M (M=O)	% PyzPz Core	% Phenoxy				
H ₂ PyzPz (6)								
H-26	-8.096		82.97	17.03				
H-23	-7.786		93.03	6.97				
H-19	-7.157		34.71	65.29				
H-7	-6.900		34.36	65.64				
H-4	-6.880		0.71	99.29				
H-3	-6.877		1.23	98.77				
H-2	-6.695		53.92	46.08				
H-1	-6.694		54.01	45.99				
номо	-5.936		94.77	5.23				
LUMO	-3.350		93.26	6.74				
L+1	-3.304		94.76	5.24				
L+2	-1.839		64.68	35.32				
L+3	-1.683		63.59	36.41				
				- 0				

of the excited state properties, the TDDFT calculations were conducted only for the diamagnetic compounds. TDDFT-predicted spectra of all macrocycles agree well with the experimental data (Fig. 1 and Supporting Information). In the case of the higher symmetry titanyl and magnesium complexes 4 and 5, TDDFT calculations predict three degenerate pairs of transitions that are responsible for the observed Q-band, ~430 nm band, and Soret band in these compounds. The first pair of the transitions (Table 2) originates from the HOMO → LUMO, LUMO+1 single-electron transitions and can be easily assigned as the traditional Q-band in the classic Gouterman's four-orbital model. According to TDDFT calculations, the ~420 nm band is dominated by the HOMO-2 → LUMO, LUMO+1 single-electron transitions. The HOMO-2 in these compounds has a_{2u} symmetry but a very different electron density distribution from the classic Goutermna's $a_{2\mu}$ orbital. More important, this orbital has a predominant (~67%) contribution from the peripheral phenoxy groups, while the LUMO and LUMO+1 are almost entirely localized at the macrocycle. Thus, this pair of transitions has a significant charge-transfer (OPh \rightarrow Pc) charge-transfer character. Finally, the third pair of intense transitions predicted by TDDFT calculations in 300-350 nm spectral envelope belongs to the Soret band and is dominated by the Gouterman's a_{2u} (HOMO-21) $\rightarrow e_{\epsilon}$ (LUMO, LUMO+1) single-electron transitions. Reduction of the effective symmetry from four-fold in the metal-containing complexes 2, 4, and 5 to two-fold in metal-free 6 results in a larger number of the allowed transitions (Table 2). Nevertheless, the Q- and Soret-bands still can be easily identified in the TDDFT calculations although the TDDFT-predicted splitting of the Q_x and Q_y bands is rather small.

Table 2. Major TDDFT-predicted excited state contributions for all compounds using the MO6 exchange-correlation functional in the gas phase.

Excited state	λ (nm)	E (cm ⁻¹)	Osc. Str., f	% Contributions	Assignment
				Ti(O)PyzPz (2)	
1, 2	593	16876	0.3375	$H \rightarrow L/L+1 (81\%)$	Q-band
9, 10	429	23336	0.4553	$H-2 \rightarrow L/L+1 (79\%)$	CT
58, 59	332	30143	0.5918	$\text{H21} \rightarrow \text{L/L+1} (56\%)$	Soret band
				MgPyzPz (5)	
1, 2	584	17131	0.3941	$H \rightarrow L/L+1 (90\%)$	Q-band
8, 9	419	23869	0.4481	$H-2 \rightarrow L/L+1 (81\%)$	CT
56, 57	327	30625	1.257	$H-21 \rightarrow L/L+1 (72\%)$	Soret band
				H_2 PyzPz (6)	
1	584	17097	0.3603	$H \rightarrow L+1 (87\%)$	Q _x -band
2	579	17263	0.4161	$H \rightarrow L (90\%)$	Q _y -band
7	412	24284	0.2966	$H-7 \to L+1 \ (72\%)$	CT
9	409	24418	0.5954	$\text{H7} \rightarrow \text{L}(74\%)$	CT
37	375	26671	0.2277	$H-19 \rightarrow L (90\%)$?
56	323	30945	1.34	$H-23 \rightarrow L+1 (58\%)$	Soret band
57	322	31059	0.7202	$\text{H23} \rightarrow \text{L (58\%)}, \text{H26} \rightarrow \text{L+-1 (23\%)}$	Soret band
58	321	31103	0.2385	$\text{H}26 \rightarrow \text{L+-1} (68\%), \text{H}23 \rightarrow \text{L} (19\%)$?

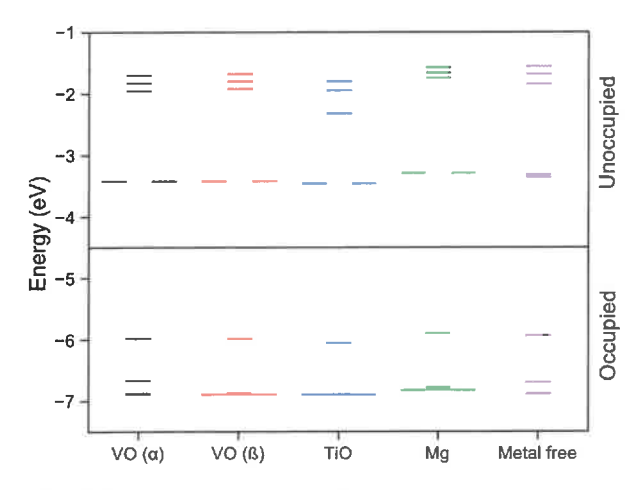


Fig. 4. DFT-predicted (M06 functional) energy diagram for the target compounds.

CONCLUSIONS

In this paper, we have discussed synthetic strategies for the preparation of titanyl and vanadyl tetrapyrazino-porphyrazines with eight 2,6-diisopropylphenoxy groups located at the peripheral positions of the macrocycle. Formation of the red-colored open-chain trimer was also observed at specific reaction conditions. The (magneto) optical spectroscopy of the new compounds reveals the expected trends although DFT and TDDFT calculations predict substantial charge-transfer (OPh \rightarrow Pc) character for the bands observed between 400 and 500 nm.

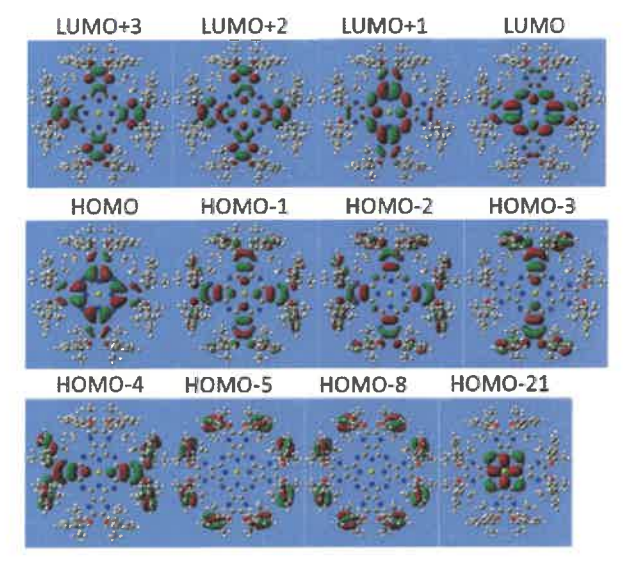


Fig. 5. DFT-predicted (M06 functional) selected frontier MOs for complex **5**.

X-ray crystal structure of the vanadyl complex $\mathbf{2}$ is very close to those published for cobalt and iron analogues and is indicative of the role of intermolecular hydrophobic interactions. Redox properties of the new compounds reveal expected trends with observable oxidation and reduction waves. EPR spectrum of complex $\mathbf{2}$ confirms its axial symmetry and the presence of the EPR-active \mathbf{d}_{xy} orbital.

Acknowledgments

Generous support from the NSF (CHE-2153081), Minnesota Supercomputing Institute, and the University of Tennessee to VN is greatly appreciated.

Supporting information

Figures S1–S20, and Tables S1-S2 are given in the supplementary material. This material is available free of charge *via* the Internet at https://www.worldscientific.com/doi/suppl/10.1142/S1088424623500050

Crystallographic data have been deposited at the Cambridge Crystallographic Data Centre (CCDC) under the number CCDC-2208789. Copies can be obtained on request, free of charge, *via* https://www.ccdc.cam.ac.uk/structures/ or from the Cambridge Crystallographic Data Centre, 12 Union Road, Cambridge CB2 1EZ, UK (fax: +44 1223-336-033 or email: deposit@ccdc.cam.ac.uk)

REFERENCES

- (a) Gregory P. J. Porphyrins Phthalocyanines 2000;
 4: 432–437. (b) Erk P and Hengelsberg H. In: Porphyrin Handbook, Kadish KM, Smith KM and Guilard R. (Eds.), Elsevier Science: San Diego, CA, 2003; Vol. 19, 105–149.
- (a) Sorokin AB. Chem. Rev. 2013; 113: 8152–8191.
 (b) Afanasiev P and Sorokin AB. Acc. Chem. Res. 2016; 49: 583–593.
 (c) Woehrle D, Baziakina N, Suvorova O, Makarov S, Kutureva V, Schupak E and Schnurpfeil G. J. Porphyrins Phthalocyanines 2004; 8: 1390–1401.
 (d) Neu HM, Zhdankin VV and Nemykin VN. Tetrahedron Lett. 2010; 51: 6545–6548.
 (e) Neu HM, Yusubov MS, Zhdankin VV and Nemykin VN. Adv. Synth. Catal. 2009; 351: 3168–3174.
 (f) Geraskin IM, Luedtke MW, Neu HM, Nemykin VN and Zhdankin VV. Tetrahedron Lett. 2008; 49: 7410–7412;
 (g) Geraskin IM, Pavlova O, Neu HM, Yusubov MS, Nemykin VN and Zhdankin VV. Adv. Synth. Catal. 2009; 351: 733–737.
- (a) Juzenas P. Trends in Cancer Res. 2005; 1: 93-110.
 (b) O'Riordan K, Akilov OE and Hasan T. Photodiagn. Photodyn. Ther. 2005; 2: 247-262.
 (c) Allen CM, Sharman WM and Van Lier JE. J. Porphyrins Phthalocyanines 2001; 5: 161-169.
 (d) Lukyanets EA. J. Porphyrins Phthalocyanines 1999; 3: 424-432.
 (e) da Silva RN, Cunha A and Tome AC. Eur. J. Med. Chem. 2018; 154: 60-67.
 (f) George L, Hiltunen A, Santala V and Efimov A. J. Inorg. Biochem. 2018; 183: 94-100.
- (a) Sekkat N, van den Bergh H, Nyokong T and Lange N. Molecules 2012; 17: 98–144. (b) Wrobel D and Dudkowiak A. Mol. Cryst. Liq. Cryst. 2006; 448: 15–38.
- (a) Gsaenger M, Bialas D, Huang L, Stolte M and Wuerthner F. Adv. Mater. 2016; 28: 3615–3645. (b)

- Liang Y, Lv W, Luo X, He L, Xu K, Zhao F, Huang F, Lu F and Peng Y. *Synth. Met.* 2018; **240**: 44–51.
- (a) Nar I, Atsay A, Altindal A, Hamuryudan E, Kocak MB and Gul A. Chem. Eur. J. 2018; 24: 6946–6949.
 (b) Woehrle D, Schnurpfeil G, Makarov SG, Kazarin A and Suvorova ON. Makrogeterotsikly 2012; 5: 191–202.
 (c) de la Torre G, Vazquez P, Agullo-Lopez F and Torres T. J. Mater. Chem. 1998; 8: 1671–1683.
- 7. (a) Nemykin VN and Lukyanets EA. In: *Handbook of Porphyrin Science*, Kadish KM, Smith KM, Guilard R. (Eds.), World Scientific Publishing Co. Pte. Ltd., Singapore, 2010; Vol. 3, pp. 1–323. (b) Lukyanets EA and Nemykin VN. *J. Porphyrins Phthalocyanines* 2010; **14**: 1–40.
- (a) Follmer AH, Ribson RD, Oyala PH, Chen GY and Hadt RG. J. Phys. Chem. A 2020; 124: 9252–9260.
 (b) Kazmierczak NP, Mirzoyan R and Hadt RG. J. Am. Chem. Soc. 2021; 143: 17305–17315.
- Engel MK. In: The Porphyrin Handbook, Kadish KM, Smith KM and Guilard R (Eds.), Elsevier Science, San Diego, USA, 2003; Vol. 20, pp. 1–242.
- 10. (a) Yamamoto S, Kuribayashi K, Murakami TN, Kwon E, Stillman MJ, Kobayashi N, Segawa H and Kimura M. Chem. Eur. J. 2017; 23: 15446-15454. (b) Majeed SA, Ghazal B, Nevonen DE, Goff PC, Blank DA, Nemykin VN and Makhseed S. Inorg. Chem. 2017; 56: 11640-11653. (c) Majeed SA, Ghazal B, Nevonen DE, Nemykin VN and Makhseed S. Dyes Pigments, 2019; 170: 107593. (d) Ghazal B. Azizi K, Ewies EF, Youssef ASA, Mwalukuku VM, Demadrille R, Torres T and Makhseed S. Molecules, 2020; 25: 1692. (e) Zimcik P, Novakova V, Kopecky K, Miletin M, Kobak RZU, Svandrlikova E, Váchová L and Lang K. Inorg. Chem. 2012; 51: 4215-4223. (f) Dini D, Hanack M, Egelhaaf H-J, Sancho-Garcia JC and Cornil J. J. Phys. Chem. B 2005; 109: 5425-5432.
- (a) Bezzu CG, Helliwell M, Warren JE, Allan DR and McKeown NB. Science, 2010; 327: 1627–1630. (b) McKeown NB. J. Mater. Chem. 2010; 20: 10588–10597. (c) Bezzu CG, Kariuki BM, Helliwell M, Tuna F, Warren JE, Allan DR and McKeown NB. CrystEngComm, 2013; 15: 1545–1550. (d) Makhseed S, Ibrahim F, Samuel J, Helliwell M, Warren JE, Bezzu CG and McKeown NB. Chem. Eur. J. 2008; 14: 4810–4815.
- 12. Gaussian 16, Revision B.01, Frisch MJ, Trucks GW, Schlegel HB, Scuseria GE, Robb MA, Cheeseman JR, Scalmani G, Barone V, Petersson GA, Nakatsuji H, Li X, Caricato M, Marenich AV, Bloino J, Janesko BG, Gomperts R, Mennucci B, Hratchian HP, Ortiz JV, Izmaylov AF, Sonnenberg JL, Williams-Young D, Ding F, Lipparini F, Egidi F, Goings J, Peng B, Petrone A, Henderson T, Ranasinghe D, Zakrzewski VG, Gao J, Rega N, Zheng G, Liang W, Hada M, Ehara M, Toyota K, Fukuda R,

- Hasegawa J, Ishida M, Nakajima T, Honda Y, Kitao O, Nakai H, Vreven T, Throssell K, Montgomery JA Jr, Peralta JE, Ogliaro F, Bearpark MJ, Heyd JJ, Brothers EN, Kudin KN, Staroverov VN, Keith TA, Kobayashi R, Normand J, Raghavachari K, Rendell AP, Burant JC, Iyengar SS, Tomasi J, Cossi M, Millam JM, Klene M, Adamo C, Cammi R, Ochterski JW, Martin RL, Morokuma K, Farkas O, Foresman JB, Fox DJ. *Gaussian, Inc.*, Wallingford CT, 2016.
- Staroverov VN, Scuseria GN, Tao J and Perdew JP. J. Chem. Phys. 2003; 119: 12129–12137.
- 14. Tao JM, Perdew JP, Staroverov VN and Scuseria GE. *Phys. Rev. Lett.* 2003; **91**: 146401.
- 15. Wachters AJH. J. Chem. Phys. 1970; 52: 1033-1036.
- 16. McLean AD and Chandler GS. *J. Chem. Phys.* 1980; **72**: 5639–5648.
- Zhao Y and Truhlar DG. Theor. Chem. Acc. 2008;
 120: 215–241.
- 18. Tenderholt AL. *QMForge*, version 2.1; Standord University: Stanford, CA, 2011.
- Palatinus L and Chapuis G. J. Appl. Cryst. 2007; 40: 786–790.
- 20. Sheldrick GM. Acta Cryst. 2008; A64: 112-122.
- 21. Betteridge PW, Carruthers JR, Copper RI, Prout K and Watkin DJ. J. Appl. Cryst. 2003; 36: 1487.
- 22. A. L. Spek 2005 A Multipurpose Crystallographic Tool. Utrecht University. Utrecht. The Netherlands

- 23. Novakova V, Zimcik P, Miletin M, Vujtech P and Franzova S. *Dyes Pigments* 2010; **87**: 173–179.
- 24. (a) Stillman MJ. In: Handbook of Porphyrin Science, Kadish KM, Smith KM, Guilard R. (Eds.); World Scientific Publishing Co. Pte. Ltd.: Singapore, Singapore, 2011; Vol. 14, pp. 461–524. (b) Mack J and Stillman MJ. In: Porphyrin Handbook, Kadish KM, Smith KM, Guilard R. (Eds.); Elsevier Science: San Diego, CA, 2003; Vol. 16, pp. 43–116. (c) Mack J, Stillman MJ and Kobayashi N. Coord. Chem. Rev. 2007; 251: 429–453. (d) Cook MJ, Dunn AJ, Howe SD, Thomson AJ and Harrison KJ. J. Chem. Soc., Perkin Trans. 1, 1988; 1: 2453–2458.
- (a) Belosludov RV, Nevonen D, Rhoda HM, Sabin JR and Nemykin VN. J. Phys. Chem. A 2019; 123: 132–152.
 (b) Martynov AG, Mack J, May AK, Nyokong T, Gorbunova YG and Tsivadze AYu. ACS Omega 2019; 4: 7265–7284.
 (c) Kobayashi N, Ogata H, Nonaka N and Luk'yanets EA. Chem. Eur. J. 2003; 9: 5123–5134
 (d) Ziegler CJ, Sabin JR, Geier III GR and Nemykin VN. Chem. Commun. 2012; 4743–4745.
- (a) Gouterman M. J. Mol. Spectr. 1961; 6: 138-163.
 (b) Gouterman M, Wagniere G and Snyder LC. J. Mol. Spectr. 1963; 11: 108-127.
 (c) Weiss C, Kobayashi H and Gouterman M. J. Mol. Spectr. 1965; 16: 415-450.